Study of the SCIDAR concept for adaptive optics applications

A.A. Tokovinin

March 26, 2002

1 Introduction

Rapid developement of adaptive optics (AO) systems has been made possible through deep understanding of optical turbulence effects. It is now clear that for the optimization of AO operation a rather complete knowledge of optical propagation parameters is needed, in particular the altitude distribution of C_n^2 must be known. The applicability of the SCIDAR technique for this purpose is studied here. A stand-alone system capable of measuring the C_n^2 profile (hereafter - profile) at any given instant during night time is considered.

In Sect. 2 we describe the principle of the technique and determine the most important system parameters. A detectivity analysis is given in Sect. 3, and the availability of suitable target stars is discussed in Sect. 4. These considerations lead to the specification of major system components which is given in Sect. 5. Sect. 6 contains our conclusions and a brief review of alternative approaches.

2 The principles of SCIDAR and Generalised SCIDAR

The principles of SCIDAR are described in [1,2]. Recently the Generalized SCIDAR (GS) was proposed [3]: instead of focusing on the telescope pupil, the detector is displaced so that the scintillation from the lowest atmospheric

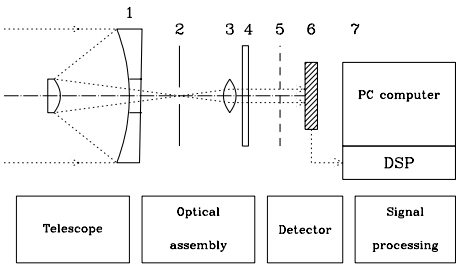

Figure 1: Optical scheme of SCIDAR. The reflecting telescope 1 forms image of a double star in the focal plane with field stop 2. The beam is then collimated by a lens 3, passes through the filter 4 and falls on the detector 6, which is placed some distance behind the exit pupil plane 5 (in GS mode) or in the pupil plane (CS mode). Detector signal is processed by computer 7 with digital signal processor (DSP) board inside.

layers becomes measurable. The GS will be considered here, because the classical SCIDAR (CS) is just a particular case of GS.

The scheme of SCIDAR is given in the Fig. 1. The whole instrument consists of the folowing major components:

1. Telescope
2. Optical assembly
3. Detector
4. Signal processor
5. Computer
6. Software

The SCIDAR operation resumes in the following. Telescope is pointed on a bright double star with angular separation θ of $3'' - 10''$. The images of atmospheric shadow bands (or speckle) produced by the turbulence are

taken by the detector with short exposure time (typically 1 ms). The auto-correlation (AC) of these images is computed in real time and averaged over integration time (typically 1 min). The normalized AC of double star $C(\vec{r})$ is computed as

$$C(\vec{r}) = \overline{I(\vec{r}_1)I(\vec{r}_1+\vec{r})}/\overline{I}^2, \tag{1}$$

where $I(\vec{r})$ is the intensity distribution over telescope pupil. The statistical averaging is performed over space (vector $\vec{r}_1$) and time. The AC of double star contains 3 terms:

$$C(\vec{r}) = \int_0^{h_{max}} C_n^2(h)[A\,C_0(\vec{r},h) + B\,C_0(\vec{r}-\theta h,h) + B\,C_0(\vec{r}+\theta h,h)]\mathrm{d}h, \tag{2}$$

where $C_0(\vec{r},h)$ is the AC produced by a single turbulent layer at altitude h with $C_n^2 = 1$. The coefficients A and B depend on the intensity ratio $\alpha = 10^{-0.4\Delta m}$ of double star components:

$$A = (1+\alpha^2)/(1+\alpha)^2; \quad B = \alpha/(1+\alpha)^2 \tag{3}$$

In the most favorable case of $\Delta m = 0$ we have $A = 0.5$ and $B = 0.25$.

The two last terms in Eq.2 contain the useful information on the $C_n^2(h)$ profile: they are proportional to the profile itself convolved with C_0 (strictly speaking it is not a convolution because the kernel C_0 depends on h). The equivalent width of C_0 is $L = 0.70\sqrt{\lambda h}$, and it defines the intrinsic altitude resolution of SCIDAR which is equal to L/θ (2.5 km for $\theta = 4''$, $h = 10$ km and $\lambda = 0.5$ nm).

The Eq.2 is valid for a source at zenith. At non-zero zenith distance z the scintillation increases as $\cos z^{-11/6}$ [8], and the distance of a turbulent layer from the telescope increases as $\cos z^{-1}$. Thus, h in Eq.2 must be in fact replaced by $h\mathrm{sec}z$. Consequently, with a star of given separation away from zenith, still larger telescope is required to reach a given altitude. At the same time the vertical resolution increases as well. Also, the small-perturbation approximation is no longer valid for $z > 60^o$ [8], so large z must be avoided to ensure correct data interpretation.

The classical SCIDAR (CS) is insensitive to low-altitude turbulence for two reasons: i) the function $C_0(\vec{r},0) = 0$, and ii) the terms in Eq.2 begin to overlap for $\theta h < L$. In the GS, the virtual observing plane can be placed

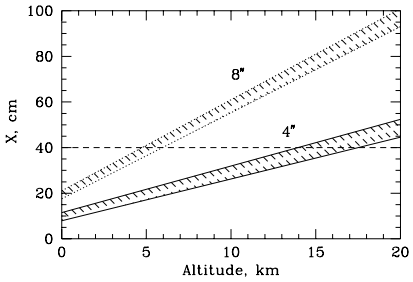

Figure 2: Displacement x of autocorrelation peaks in function of altitude and double star separation in a GS with altitude offset $H_0 = -5$ km. The width of shaded bands depicts the FWHM of the correlation. The autocorrelation at $x = 40$ cm (horizontal line) corresponds to different altitudes for double stars of different separations, and altitude resolution is also different.

at some altitude $-H_0$ below the ground, and the physical altitude H of a turbulent layer is replaced in Eq.2 by $h = H - H_0$. (It is possible to make H_0 positive, but this case is of little practical interest and will not be considered here.) Altitude offset H_0 can be optimized; in the following, we will assume $H_0 = -5$ km, so that the terms in Eq.2 are safely separated even for ground layers.

To measure the turbulence at altitude h, we must measure the AC for displacement $x = \theta h$. In Fig.2 $x(h)$ is plotted for various double star separations θ. The width of the shading depicts the width of AC. If a wider double star is selected, the altitude resolution increases, but larger telescope is required. Unfortunately, the choice of available stars is very limited, and we have to work with separations as large as $10''$ (see below). Thus, a telescope diameter of at least $D = 1.2$ m is required to measure the profile up to $H = 20$ km. Larger telescope also provides better detectivity.

If we were free to select a double star separation for a given telescope that would provide highest altitude resoltion while reaching the maximum specified altitude, the number of resolution elements in the profile could be

estimated as $N_{max} = D/0.7\sqrt{\lambda H_0}$. In the real life the number of resolution elements will always be less than N_{max}.

Focusing the detector on the virtual plane which is not coincident with pupil plane introduces diffraction near pupil edge. The width of this zone is about $\sqrt{\lambda H_0}$. In the edge zone the scintillation intensity is distorted, and must not be used in calculation. So, in a GS the effective pupil diameter is reduced by $2\sqrt{\lambda H_0} = 8$ cm for $H_0 = -5$ km. Similarly, the pupil zone near the shade of secondary mirror and spiders must be avoided in GS.

The characteristic size of scintillation pattern produced by the turbulence at the distance $H_0 = -5$ km is equal to $0.7\sqrt{\lambda H_0} = 3.5$ cm, and somewhat larger at greater altitudes. To sample this pattern with 2 detector pixels, we choose pixel size of 2 cm. The number of photons received being very limited, pixel size can not be reduced without loss of detectivity, so the adopted pixel size of 2 cm must not be considered as a free parameter.

The scintillation pattern moves across the pupil with effective wind speed. Taking it to be 20 m/s (or 72 km/h), in 1 ms exposure time the pattern will be smeared by just 2 cm, which is barely noticeable. The experience of J. Vernin group shows that in some extreme situations (wind up to 50 m/s) the exposure times as short as 0.5 ms may be required to "freeze" the scintillation. However, in the following we adopt exposure time of 1 ms which is likely to be used most of the time.

If the scintillation image produced by a single star is correlated with delayed image, the peak in AC that corresponds to a particular turbulent layer is displaced. The amount and direction of displacement are directly related to the wind speed of a layer. Thus, a possibility exists to measure the wind velocity in upper atmosphere with SCIDAR, as demonstrated in [2]. However, there is yet no general solution which permits to extract wind profile from such data: the problem is evidently related to the fact that displaced peaks in the cross-correlation can overlap. It is not excluded that a method of wind extraction profile be elaborated in the near future. For the moment, we do not consider GS as an instrument for wind profile measurement. A system studied here can however be used for wind profile measurement when a suitable data processing technique becomes available, because no additional hardware components are needed for cross-correlation computing.

The scintillation pattern is caused by diffraction of light waves, and thus is wavelength-dependent. The chromatic decorrelation was studied in [1]: for a bandwidth of $\Delta\lambda/\lambda = 0.25$ which corresponds roughly to the unfiltered S20

photocathode spectral response the correlation remains as high as 86%. This loss will be larger for a wider bandwidth, but in principle it can be taken into account in the data processing.

A more serious problem which forbids the use of large spectral bandwidth is related to the chromatic refraction. The angular distance between red and blue stellar images for a zenith distance z is approximately equal to $1''\mathrm{tg}z$. Thus, a layer at 20 km would give red and blue speckle patterns smeared by 10 cm at the telescope pupil for $z = 45^o$ (in fact thisdisplacement will be less because most of refraction occurs at lower altitudes). This smearing is comparable to the Fresnel speckle size and somewhat degrades the altitude resolution when double star components happen to be viewed in the vertical direction. In the following we assume that zenith distance will not exceed 45^o.

The possibility of increasing the scidar altitude resolution by deconvolution is sometimes discussed (it must be noted that Eq.2 is not a convolution, but a Fredholm Type 1 integral equation, of which a normal convolution is just a specific case). J. Vernin and his collaborators routinely use the maximum entropy technique which seems to take advantage of the inherent profile positivity and its typical multi-peaked shape. A gain of 2 can be thus achieved in the vertical resolution for good S/N data. However, the S/N ratio in the input data may be very low, and it is known that in these conditions no considerable gain in resolution is possible by aposteriory data processing. We do not consider here any deconvolution techniques, assuming that their eventual use will not change major system characteristics.

3 Detectivity analysis

As explained above, the output of SCIDAR is a $C_n^2(h)$ profile convolved with instrumental response function. In what follows the smoothed C_n^2 are thus considered. The profile is estimated from the autocorrelation function accumulated during the time T. The rms error of C_n^2 depends on the error of AC measurement. It was estimated in [2]. Here we repeat this derivation with the following generalizations:

1. It is known that optical turbulence is usually concentrated in very thin

layers. The strength of each layer is characterized by the integral

$$J = \int_{layer} C_n^2(h)\mathrm{d}h, \ [\mathrm{m}^{1/3}] \tag{4}$$

which is called *turbulent optical factor* and is directly comparable to the integrated effect of optical propagation through whole atmosphere (for $r_0 =$ 20 cm at $\lambda = 500$ nm $J = 2.19 \cdot 10^{-13}\mathrm{m}^{1/3}$).

Accordingly, the detectivity in terms of J is estimated. The corresponding error on C_n^2 is then obtained by dividing the error on J by the vertical resolution (see formulae below). Both errors have different dependence on altitude.

2. The number of spatial samples of correlation function is estimated as $\sqrt{s/S(x)}$, where $s = 0.355\lambda h$ is the scintillation coherence area [2], and $S(x) = 2S_0/\pi(\arccos\epsilon - \epsilon\sqrt{1-\epsilon^2})$ is the overlap area of pupil shifted by $x = \theta H$ ($\epsilon = x/D$, $S_0 = \pi D^2/4$). In case of GS, the physical altitude H must still be used here, and not the virtual altitude h, because additional altitude offset H_0 provokes only pupil displacement on the detector but does not reduce the number of correlated speckles. The dependence of spatial samples number on x was not taken into account in [2], but it is important when x is comparable to D.

3. In [2] the statistical speckle noise only was considered. However, for faint stars the photon noise and detector readout noise become important. The problem of estimating the image correlation function in the presence of photon and detector noise is well known in speckle interferometry. The speckle noise term ($C_{**}(0)$ in notation of [2]) must be replaced by the sum of noise dispersions due to speckle, photon and readout noise. Photon noise is equal to $0.25/\delta$, and readout noise is equal to $0.5(n/\delta)^2$, where δ is the mean number of photons per pixel detected in each exposure and n is the rms readout noise in electrons. The speckle term $C_{**}(0) = A\sigma_I^2$ is related to the usual scintillation index for single star $\sigma_I^2 = \overline{\Delta I^2}/\overline{I}^2$ (scintillation produced by all atmospheric layers), while A (Eq.3) takes into account the source binarity.

The calculation of errors on J and C_n^2 is given in the Appendix, and final results are:

$$\Delta J = \frac{A\sigma_I^2 + 0.25/\delta + 0.5(n/\delta)^2}{2.25Bk^{7/6}h^{5/6}}\sqrt{\frac{s\tau_c}{TS(x)}}, \ [\mathrm{m}^{1/3}] \tag{5}$$

$$\Delta C_n^2 = \Delta J / \sqrt{0.355 \lambda h}, \tag{6}$$

$$\Delta C_n^2 = \theta \frac{A\sigma_I^2 + 0.25/\delta + 0.5(n/\delta)^2}{3.96 B k^{2/3} h^{4/3}} \sqrt{\frac{s\tau_c}{TS(x)}}, \ [\mathrm{m}^{-2/3}]. \tag{7}$$

where $k = 2\pi/\lambda$. Eq.7 is very similar to the formula (34) in [2]. The parameter τ_c is time interval between successive frames.

It can be noted that detectivity dependence on source magnitude and detector (via δ and n), on one hand, and on altitude and telescope, on the other hand, are combined in a multiplicative manner, and so can be analysed separately. In the following, we adopt some typical values of relevant parameters:

$\lambda = 500$ nm

$D = 1.12$ m (1.2-meter telescope reduced by edge diffraction effect)

$T = 60$ s

$\tau_c = 20$ ms (it can be as small as 1 ms, but is limited by signal acquisition and processing rate; standard TV rate is assumed)

$\sigma_I^2 = 0.1$ (this parameter is known to be highly variable, and its typical value is taken here)

$\Delta m = 1$ (more realistic than $\Delta m = 0$ and still tolerable because noise increases by only 50%)

$H_0 = -5000$ m

In calculating the photon flux, we assume pixel size of 2 cm (as related to pupil plane) and exposure time of 1 ms. The wavelength band of 100 nm is also assumed. Combined transmission of atmosphere, telescope and optical assembly is taken to be 0.5.

Two detectors are considered: the intensified CCD (ICCD) with quantum efficiency of 10% and no readout noise, and fast CCD with quantum efficiency of 50% and readout noise of 1 and 4 electrons. In the latter case, the number of photons $\delta = 10$ for a combined source magnitude 5.

In Fig. 3 the ΔC_n^2 is plotted versus source combined magnitude for $h = 10$ km and $\theta = 4''$. The advantage of CCD over ICCD in the relevant magnitude range is evident. The readout noise of CCD detector affects the detectivity for faint sources, where the performance of both detectors becomes comparable. The performance is similar for bright sources, too, where the speckle noise dominates photon noise. On the other hand, detectivity depends on σ_I^2, i.e. on the profile itself: for a stronger turbulence noise is also stronger.

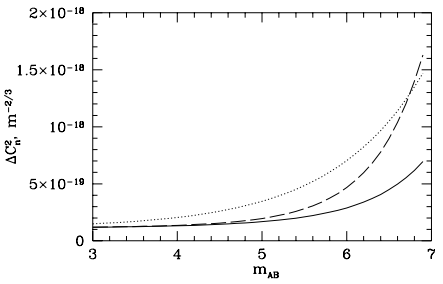

Figure 3: Error ΔC_n^2 at $h = 10$ km for double star with $\theta = 4''$ and $\Delta m = 1$ for different detectors: CCD with readout noise 1 e^- (full line), CCD with readout noise 4 e^- (dahsed line) and ICCD (dotted line), in function of the combined source magnitude m_{AB}.

Detectivity of GS is lower than that of CS because the total scintillation is increased for $H_0 < 0$. In situations with high wind speed the exposure time will be reduced to 0.5 ms, which is equivalent to the 2 times flux loss: the curves on Fig. 3 will be displaced 0.75^m to the left.

The dependence of detectivity on altitude and double star separation is illustrated in Figs. 4 and 5. The calculations are made for a star of magnitude 5 and a CCD detector with 1 e^- readout noise. From Fig. 4 is is clear that ΔC_n^2 is proportional to θ: for larger θ the altitude resolution is increased, and the profile is spread in more AC pixels. The effect of reduced number of spatial samples is very pronounced for $\theta = 8''$, but it will be much less for larger telescope aperture.

As shown in Fig. 5, the ΔJ is practically independent on h and θ. Although the scintillation produced by a given layer is stronger at higher altitudes, this is almost entirely compensated by resolution decrease and reduced number of spatial samples. A given layer produces a peak in the AC of the same width, independent of θ. This is why the layer detectivity depends on θ only weakly via spatial sampling term. Here again, this dependence will be much less for a telescope of larger size. The turbulent layer with

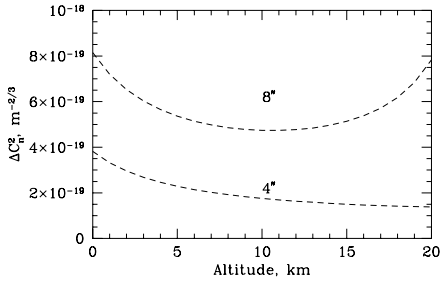

Figure 4: Dependence of C_n^2 error on altitude for double stars with separations $4''$ and $8''$. A CCD detector with 1 e^- readout noise is assumed. Telescope diameter $D = 1.2$ m, combined source magnitude $m_{AB} = 5$.

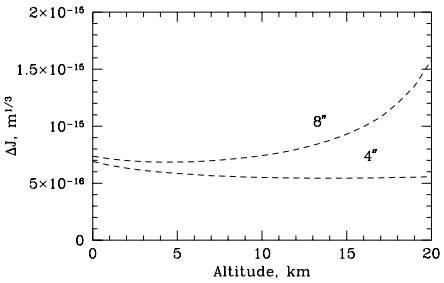

Figure 5: Altitude dependence of "layer" detectivity ΔJ for the same instrument parameters as in Fig. 4.

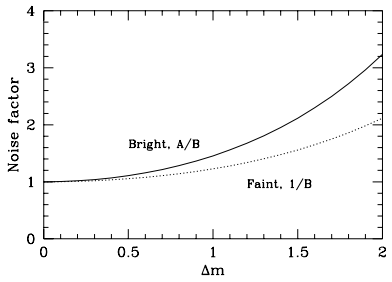

Figure 6: Relative noise increase in function of magnitude difference for bright and faint sources.

$J = 1 \cdot 10^{-15}\mathrm{m}^{1/3}$ contributes some 0.5% to the total seeing at a good site ($r_0 = 20$ cm), so the detectivity seems adequate.

The noise dependence on source magnitude difference enters via the factors A and B. Noise is proportional to A/B for bright sources ($\delta >> 1$) and to $1/B$ for faint sources where photon and readout noise dominate speckle noise. In Fig. 6 the normalised noise increase is plotted against Δm for both cases (the real situation is somewhere in between). As stated above, magnitude difference up to 1^m or slightly more is acceptable.

The possible ways of improving the detectivity are listed below:

1. Increase of integration time T reduces noise as $T^{-1/2}$.

2. Increase of telescope diameter reduces noise at least as D^{-1}, and much more in the poor spatial-sampling case (when $\theta H \approx D$).

3. Frame rate τ_c can be increased up to 20 times, because it is limited by signal acquisition and processing speed. Photon and readout noise can thus be reduced by 5 times. The reduction of speckle noise would be less because speckles in consequtive 1 ms exposures would remain partially correlated.

4. For ICCD detector the bandwidth is limited by the photocathode spectral sensitivity, and no additional filter is used. On the other hand, the good sensitivity of direct CCD in the red and NIR encourages to increase bandwidth and to use $\lambda > 500$ nm. However, noise also increases as $\lambda^{7/6}$ or

$\lambda^{2/3}$ (Eqs. 5,7). If no filter is used in front of a CCD, the detectivity would be the highest, but the effective λ and bandwidth would depend on the source spectral type. This must be properly taken into account in signal processing. Also, for large zenith distance the vertical resolution would be degraded by chromatic refraction. We recommend to limit the band to 100 nm by a filter.

4 List of double stars

The computer version of the Washington Double Star catalogue (WDS) [5] which contains some 70000 entries was scanned. Different selection criteria were tried. It turns out that the total (whole-sky) number N of double stars with both components brighter than a given visual magnitude m in the separation range from ρ_1 to ρ_2 arcseconds can be estimated by the formula

$$N = 10^{0.43m-0.47}(1/\rho_1 - 1/\rho_2). \quad (8)$$

For example, the formula predicts that there are only 20 sources with both components brighter than 6^m and separation $4''-10''$ (actually, the number of such sources is 16). The inverse proportionality of source number on angular distance must be noted: it is easier to find closer double stars!

The final selection of southern double stars with separations from $2.5''$ to $10''$, with both components brighter than 7.5^m and magnitude difference less than 1.5^m is given in the Table. Some manual editing was needed to delete stars with multiple components of comparable brightness.

In the WDS the first and last measurements of ρ are usually given down to $\pm 0.1''$. We calculated the rate of distance change in arcseconds per year and extrapolated the distances to the epoch 2000.0. These extrapolated distances are listed in the Table, together with rate and the year of last measurements. For a few systems with computed orbits we used the orbital elements instead to compute the predicted position for 2000.0 and the rate (*orb* in the "last year" column). The only exception is HR 7948, for which a very long-period and probably wrong orbit predicts a constant separation of $13.77''$, incompatible with recent measurements.

The objects were identified with the catalogue of Bright Stars (BS) [6], and the HR numbers of the primary/secondary components are also given. We took from BS the equatorial coordinates for 2000.0 (in the format $hh.mmss$ for right acsention and $dd.''''$ for declination), the photoelectric V-magnitudes

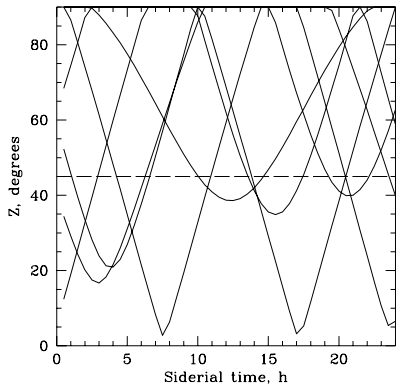

Figure 7: Zenith angle of the selected SCIDAR target stars in function of local siderial time. Dashed line indicates the adopted limit $z < 45^o$.

of both components and spectral type of the primary. Combined magnitudes V_{AB} are calculated. For some systems the components are listed under a single HR number, and separate photometry is not available; individual magnitudes are then taken from WDS and given with one decimal, the combined magnitudes are still from BS. A few sources have components of significantly different colors (HR 1212, 1771, 4652, 6730).

In the "*" column the recommended sequence of best sources that provide continuous sky coverage is given. By far the best SCIDAR target is HR 4730/31 = α Cru. For these sources the zenith angles were calculated for any local siderial time ST (fig. 7). The duration and position of dark night time with respect to the ST changes during the year. Continuous coverage is provided when at least 1 source is available at any given instant of ST. It can be seen that most of the time there are at least 2 sources.

The strategy of target selection may be developed given the source list and the preferences. For example, if at any given moment the brightest target above 45^o is selected, we obtain the dependence of combined magnitude and separation on ST (Fig. 8). It can be seen that the separations and magnitudes vary significantly, with attendant variation of resolution and detectivity. If z up to 50^o is admissible, the target selection is easier and the faintest source in Fig.8 (HR 9002) can be avoided.

Table 1: List of SCIDAR target double stars in the southern hemnisphere

R.A.	Dec.	V_{AB}	V_A	V_B	ρ, $''$	$\dot{\rho}$	Last	*	HR	Sp.(A)
1.5332	19.1737	4.04	4.75	4.83	7.63	-0.005	1969		546/45	A1p
2.5816	-40.1817	2.91	3.24	4.35	8.32	0.001	1975	*	897/98	A4III
3.4836	-37.3714	4.26	4.73	5.40	8.13	0.005	1975		1190/89	B9V
3.5417	-2.5717	3.97	4.79	4.65	6.80	0.000	1966	*	1212/13	G8III
5.2146	-24.4623	4.70	5.06	6.09	3.53	0.002	1983		1771/72	G7II+A7
7.2021	-52.1842	5.54	6.05	6.60	9.05	-0.006	1960		2813/14	F0IV
7.2851	-31.5054	5.94	6.38	7.13	8.90	0.000	1968		2870/71	B3V
7.3419	-23.2825	5.10	5.83	5.87	9.68	0.002	1965		2909/10	dF4
7.3849	-26.4806	3.81	4.50	4.62	9.90	0.000	1964	*	2948/49	B6V
9.1231	-43.3649	5.57	6.2	6.9	2.80	0.000	1977		3661	B8Vp
9.3046	-31.5322	5.76	6.18	7.00	8.00	0.000	1977		3781/80	A0V
10.1958	19.5030	2.30	2.61	3.80	4.41	0.003	**orb**		4057/58	K1III
11.3216	-29.1540	4.97	5.64	5.81	9.30	0.000	1967		4444/43	F8V
12.1403	-45.4326	4.92	5.31	6.22	2.80	0.000	1963		4652/53	K3III
12.2636	-63.0557	0.76	1.33	1.73	4.01	-0.009	1979	*	4730/31	B0.5IV
12.4116	-13.0054	5.28	5.98	6.08	5.40	0.000	1980		4822/21	F5V
13.4145	-54.3336	5.01	5.7	7.1	5.40	0.000	1963		5141	B8Vn
13.5150	-32.5940	4.32	4.56	6.06	7.82	-0.003	1975		5210/11	B5IIIp
14.2323	8.2648	4.92	5.12	6.86	6.22	0.001	1973		5386/85	A0V
14.4044	16.2506	4.56	4.94	5.88	5.57	-0.001	1977		5475/76	B9p
15.3448	10.3221	3.05	3.80	3.80	4.29	0.008	**orb**	*	5789/88	F0IV
16.2440	-29.4217	5.41	5.84	6.63	4.60	-0.018	1966		6106/05	G0IV
16.2535	-23.2650	4.63	5.02	5.92	2.94	-0.007	1975		6112/13	B2IV
17.1521	-26.3605	4.34	5.07	5.11	4.91	0.015	**orb**	*	6402/01	K0V
18.0130	21.3544	4.31	4.96	5.18	6.33	0.001	1974		6730/29	A5IIIn
18.4528	5.2959	5.83	6.2	6.6	2.54	0.002	1979		7048	A1V+A1V
20.4640	16.0727	3.87	4.27	5.14	9.22	-0.016	1976	*	7948/47	K1IV
21.0405	-5.4923	5.63	5.89	7.31	2.46	-0.001	1973		8059/58	G4III
22.1418	-21.0427	5.32	5.7	7.2	5.10	0.000	1975		8480	K0III+F2
23.0715	-50.4111	5.83	6.1	6.8	8.81	0.004	1975		8793	F6IV-V
23.4601	-18.4041	5.29	5.8	6.8	6.78	0.007	1975	*	9002	F2III+F2

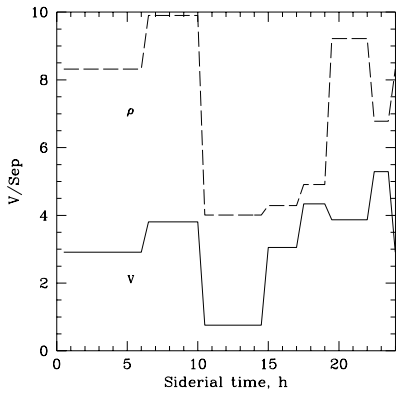

Figure 8: The combined visual magnitude V (full line) and angular separation (dashed line) of the brightest SCIDAR target with $z < 45^o$ against local siderial time.

The source selection strategy depends also on the desired system parameters. It may happen that the maximum altitude is limited by a telescope size for a too wide double star. Then a closer star may be selected to measure the high-altitude turbulence with reduced resolution, and then a wider star will be used to measure the low and medium altitude turbulence with better resolution. This is why it is important to have a redundant source list.

5 System specifications

The specifications on system components are given here after some practical considerations. It is assumed that C_n^2 profile must be measured at any given moment during the night without human assistance. Maximum altitude is 20 km, altitude resolution is 1-2 km, depending on the source.

A major issue in defining system parameters is the choice between classical and generalized modes of operation, CS and GS respectively. Both CS and GS look very similar, but the system parameters are different:

i) GS requires a telescope with reasonably good optical quality ($1''$ FWHM or less) and good tracking accuracy. This strict tolerance is because GS uses the image-forming capability of a telescope. Telescope aberrations become

visible in the defocused pupil image, and they must be less than random atmospheric aberrations. A CS is in principle insensitive to telescope aberrations. The only potential problem is a sky background: for a worst-case background of 16^m per sqare arcsecond (full-moon sky) the sky flux in a $60''$ aperture is equivalent to a 7.37^m star, i.e. the background would contribute 28% of the flux for a 6^m target. Thus optical quality specification for a CS is $1'$.

ii) The tracking accuracy of $\pm 5''$ or better is needed for GS, because defocused pupil moves on the detector when source is displaced in the field. With $H_0 = -5$ km the image displacement due to tracking errors would be ± 12 cm, or 6 pixels. Source position in the field can be updated between exposures, so tracking error must not exceed the limit only during data acquisition (say, 10 min). On the other hand, CS may have much greater tracking errors, because pupil image on the detector is stable.

iii) The GS has a reduced detectivity in comparison with CS, because the lower layers with strong turbulence contribute to the scintillation, increasing σ_I^2. It is difficult to estimate the exact amount of detectivity loss, because it depends on C_n^2 profile and on the choice of H_0.

iv) A maximum altitude of GS is slightly less than that of CS, due to pupil edge diffraction.

In what follows we list the system specifications for CS:

1. Telescope with mirror diameter $D = 1.2$ m. Telescope can be the most expensive part of the whole system.

Optical quality: FWHM image size on axis of $30''$ or less.

Tracking errors of $\pm 30''$ or better during 10 minutes. A simple autoguider option may be considered.

Blind pointing accuracy of $1'$ for initial source acquisition in the field. Precise source positioning can be made with the help of SCIDAR detector.

Telescope operation (pointing, dome and mirror opening and closure, focusing) must be remotedly controlled by a computer.

The considerable experience in automated telescope design and operation has been accumulated by the Automated Photometric Telescope group which has a facility on Mt. Hopkins (Arizona). A complete automatic telescope may be purchased there.

2. Optical assembly is rather simple and inexpensive. In its simplest form it must contain a positive lens, filter and field stop (Fig. 1). The focal length f of a lens is chosen in function of telescope effective focal length F

so that a detector pixel must project to 2 cm at the pupil. With pixel size of 20 μm a demagnification $G = 1000$ is needed. With $F = 10$ m we have $f = F/G = 1$ cm. A 1.2 m pupil will project on 60 detector pixels, or 1.2 mm. The displacement of detector from the pupil plane is equal to H_0/G^2, or 5 mm for $H_0 = 5$ km.

For pointing it is desirable to have a $1'$ field image on the detector. It can be obtained if a lens of 4 mm focal length is inserted in the parallel beam just in front of the detector (for $G = 1000$). At the same time the field stop in the focal plane must be removed. So, the optical assembly must provide for remotedly-controlled in-out motion of additional acquisition lens. If for reasons of insufficient space it will be difficult to insert additional lens in front of a detector, the whole optical train including field stop, lens and filter may be removed from the beam and replaced by acquisition train with field re-imaging lens and, possibly, a neutral density filter.

3. Detector of choice is a fast-readout CCD with low readout noise (less than 2 e^-). Minimum number of pixels is 64x64. Pixel size is irrelevant (only f depends on it). It is important that exposures as short as 0.5 ms can be realized, and that exposure start and end be synchronous for all pixels. If short and synchronous exposure can not be realized by the detector itself, a mechanical shutter is necessary. It may be a rotating-sector type shutter in the focal plane, with a slit of variable width. CCD readout and shutter rotation must be synchronized. If the frame acquisition rate is limited by signal processing speed, the detector readout need not be made in 1 ms, but can take up to 20 ms. This may help to reduce readout noise.

Intensified CCD can also be used, with some loss of detectivity (Fig. 3). In this case an electronic shutter must control the intensification stage. The problem of intensifier reminicence exists, so the phosphor must be a rapid one with decay time of few milliseconds. If ICCD is chosen, the maximum possible photocathode quantum efficiency is imperative.

4. Signal processor digitizes the video signal from the detector, computes the autocorrelation (AC) function on 64x64 pixels (as well as some additional quantities to take into account flat field and bias non-uniformity, see [7]) and accumulates it in the computer memory. Video signal has low information content, its digitisation into 8 bit is more than adequate (4 bits would be enough). AC calculation is done by 2D fast Fourier transform (FFT) algorithm which requires a few $(N \log_2 N)^2$ floating point operations, N being the number of pixels (a few 3.7 Mflops for 64x64 pixel format and

20 ms frame rate).

Fast real-time signal processing steps are summarized in the flow-chart below. The FFT of the autocorrelation is taken, its square modulus is computed and accumulated in real time. The inverse FFT to obtain the AC is done after end of acquisition. Also in real time the average intensity is accumulated for correction of detector non-uniformity.

$$\begin{array}{ccccccc} I(i,j) & \rightarrow & \text{FFT}, \tilde{I} & \rightarrow & \text{sq.modulus}, |\tilde{I}|^2 & \rightarrow & \text{sum}, <|\tilde{I}|^2> \\ 64\text{x}64, 8\text{bit} & & 64\text{x}64, \text{complex} & & 64\text{x}64, \text{real} & & 64\text{x}64, \text{real} \\ & & & & & \rightarrow & \text{sum}, <I> \end{array}$$

Signal processing is best done by specialized digital signal processors (DSP). They are optimized for high-speed FFT computation. For example, the DSP TMS320C30 (Texas Instruments) takes 1D FFT of real 64-pixel vector in 0.075 ms (with 60 ns processor cycle time). Thus, a 2D FFT would take 4.8 ms. More powerful DSPs exist actually on the market. It must be noted that the computing power of DSP can hardly be estimated in Mflops, because computing algorithm and data transfer optimization are equally important for fast processing.

An option for computing cross-correlation of an image with a delayed image is very desirable for eventual wind profile measurement. The delay of few ms is required, so a memory buffer of 1 frame is adequate for this task. Frame rate of 20 ms is a bit too slow for wind measurements, and must be increased to 5-10 ms. Anyway, increased frame rate is very desirable for noise reduction. An option of parallel processing with several DSP may be worth considering.

5. Computer may be a Penthium PC computer interfaced with the DSP (a DSP signal acquisition board will be placed on the computer bus). Computing power would be more than adequate for instrument control (including telescope control either directly or interfaced with dedicated telescope control computer), quick-look data analysis and data storage. A suitable medium for data archiving is necessary (DAT tape or optical disk), as well as network interface for data transfer and remote instrument control.

6. Software. The major cost of signal processing may be not the cost of DSP *per se*, but the associated cost of software developement. We suggest that J.Vernin group from the Nice University be contracted for software developement, due to their unique experience in SCIDAR data processing. The

software includes DSP programming and the extraction of C_n^2 profile from AC. Wind profile extraction software developement may also be considered.

6 Conclusions

The evaluation of SCIDAR feasibility and cost must begin with its 2 most critical components, telescope and detector. A telescope size choice is driven by required altitude resolution and, to lesser extent, required detectivity. It must also be decided whether the measurement of C_n^2 profile in the first 2 km above the ground is needed: if not, a classical SCIDAR must be preferred to GS, with attendant relaxation of telescope optical quality and tracking specifications. Once the telescope is selected, the list of target sources can be established.

The availability of fast-readout CCD must be checked, and maximum readout rate known. The necessity of a mechanical shutter in the optical assembly also depends on the detector properties.

For maximum achievable processing speed the J.Vernin group must be consulted.

Given the telescope and detector parameters and frame rate, the detectivity and altitude resolution can be calculated for each of the selected target sources.

A brief review of other possiblities to sense and measure the high-altitude turbulence must be given here. A major restriction of the SCIDAR technique comes from the use of double stars, limiting the choice of bright sources and precluding the use of small telescopes. So, alternative optical techniques which use single stars as light sources deserve some consideration.

The scintillation index σ_I^2 is known to be proportional to $\int C_n^2(h)h^{5/6}\mathrm{d}h$ for a very small telescope ($D < 2$ cm), and to $\int C_n^2(h)h^2\mathrm{d}h$ for a medium-size telescope ($D > 10$ cm) [8]. The $\int C_n^2(h)\mathrm{d}h$ can be calculated from the seeing FWHM or r_0. Thus, 3 integrated moments of $C_n^2(h)$ profile can be obtained quite easily with a small telescope, and can give a quantitative measure of the strength of high-altitude turbulence.

A generalisation of this approach consists in measuring σ_I^2 with apertures of different size and in reconstructing the profile from these data [9]. Such data must be taken simultaneously, and one can envisage a system where telescope aperture is divided in few concentric zones, with light from each

zone directed to separate detector.

A viable approach may consist in measuring the σ_I^2 in a defocused pupil plane at different H_0. Turbulent layers are thus combined with different weights, and the profile can be reconstructed by matrix inversion. The analysis of this technique in terms of resolution and detectivity has not yet been done.

A common feature of all "single-star" methods is their poor altitude resolution. However, in the worst case of "economic" SCIDAR ($D = 60$ cm) with $2.5''$ double star the altitude resolution is only 4 km, i.e. only 5 points on the $C_n^2(h)$ profile. This resolution may be comparable to single-star techniques performance, while these latter methods must be cheaper and easier to realize. The potential of SCIDAR for wind profile measurement is however difficult to rival with single star methods.

References

[1] Vernin J., Azouit M. Traitement d'image adapté au speckle atmosphérique. I. Formation du speckle en atmosphère turbulente. Propriétés statistiques. J.Optics (Paris), 1983, V. 14, P.5-9.

[2] Vernin J., Azouit M. Traitement d'image adapté au speckle atmosphérique. II. Analyse multidimensionelle appliquée au diagnostic à distance de la turbulence. J.Optics (Paris), 1983, V. 14, P. 131-142.

[3] Fuchs A., Tallon M., Vernin J. Focusing on a turbulent layer: Principle of the "Generalized - Scidar". Applied Optics, 1997, submitted.

[4] Goodman J.W. Statistical Optics. N.Y.: J.Wiley, 1985.

[5] Worley C.E., Douglass G., 1984, The Washington Double Star Catalog. U.S. Naval Obs.

[6] Hoffleit D., Warren W.H., 1991, Preliminary Version of the Bright Star Catalogue, 5th Revised Edition. NASA CD-ROM

[7] Azouit M., Vernin J. Remote investigation of tropospheric turbulence by two-dimensional analysis of stellar scintillation. J. Opt. Soc. Amer., 1980, V. 37, P.1550-1557.

[8] Roddier F. The effects of atmospheric turbulence in optical astronomy. Progress in Optics, 1981, V. 19, P.281.

[9] Ochs G.R., Ting-I Wang, Lawrence R.S., Clifford S.F. Refractive turbulence profiles measured by one dimensional spatial filtering of scintillations. Appl. Opt., 1976 V. 15, P. 2504-2510.

7 Appendix: Calculation of SCIDAR detectivity

The calculation of errors on the final quantities like the C_n^2 profile and the layer integral J consists of 2 parts. First, we evaluate the error of autocorrelation $\Delta C(\theta h)$, and then relate it to the final errors.

The rms dispersion of the speckle image autocorrelation (AC) in presence of poisson photon noise is calculated in the context of speckle interferometry [4]. For one image it is proportional to the sum of intensity dispersion and photon dispersion (in our case these are relative dispersions, because the AC is normalised by the square of mean intensity):

$$\Delta C = (C(0) + 1/K)M^{-1/2}, \tag{9}$$

where K is the mean number of photons per speckle. The first term is equal to the scintillation index $\sigma_I^2 = \overline{\Delta I^2}/\overline{I}^2$ for a single star, and must be multiplied by the factor A in case of binary star, to take into account the reduced speckle contrast (for equal components $A = 0.5$, and contrast is reduced by 0.5 due to the superposition of two similar uncorrelated speckle patterns).

As shown above, the Nyquist condition requires that there be 2x2 pixels per speckle. So, $K = 4\delta$, where δ is the number of photons per pixel.

The detector readout rms noise n (in electrons) can be taken into account as well by adding its normalized value, $0.5(n/\delta)^2$. Evidently, it is uncorrelated with both speckle and photon noise. The factor 0.5 takes care of the Nyquist sampling, as above.

The total number of speckles $M = S/s$ is equal to the ratio of image surface S to the equivalent speckle size $s = 0.355\lambda h$ (cf. [2]). Only the overlapping portion of pupil contributes to the autocorrelation for a given

shift x. Thus, $S(x) = 2S_0/\pi(\arccos\epsilon - \epsilon\sqrt{1-\epsilon^2})$, where $\epsilon = x/D$, $S_0 = \pi D^2/4$.

Finally, the total number of processed images is T/τ_c, where T is the integration time and τ_c is frame rate. The noise of the accumulated AC is estimated as

$$\Delta C = (A\sigma_I^2 + 0.25/\delta + 0.5(n/\delta)^2)\sqrt{\frac{s\tau_c}{TS(x)}}. \tag{10}$$

Now we come to the second part of the derivation. Let us consider the single turbulent layer at altitude h with C_n^2 integral equal to J. The C_n^2 profile can be approximated by the Dirac delta-function:

$$C_n^2(h_1) = J\mathrm{Dirac}(h_1 - h). \tag{11}$$

The resulting AC would contain 3 peaks, one at the origin and 2 at $\pm\theta h$. Considering only one peak at $x = \theta h$ which gives the useful information on our layer, the Eq.2 gives the AC $C(x)$ of the form

$$C(x) = JBC_0(x - \theta h, h) = JBC_0(0, h). \tag{12}$$

The integral equation kernel $C_0(\vec{r}, h)$ is given by a rather complex integral:

$$C_0(\vec{r}, h) = 8\pi k^2 0.033 \int |K|^{-11/3} \sin^2 \frac{h|K|^2}{2k} e^{-i(\vec{K}\vec{r})} \mathrm{d}\vec{K}. \tag{13}$$

For $r = 0$ the integral can be expressed through Γ-function, cf. [2], and we finally obtain

$$C_0(0, h) = 8\pi k^2 0.033 \frac{\pi^2 (k/h)^{-5/6}}{4\Gamma(11/6)\sin(5\pi/12)} = 0.25 k^{7/6} h^{5/6}. \tag{14}$$

Using Eqs.12,15 the AC error ΔC (Eq.10) can be related to the J error, leading to Eq.5. The error on C_n^2 is obtained from the error on J if we divide it by the equivalent width of $C_0(x, h)$ kernel (Eq.6), thus obtaining Eq.7.